Quaternary Geochronology 22 (2014) 175–182

Contents lists available at ScienceDirect

Quaternary Geochronology

journal homepage: www.elsevier.com/locate/quageo

Research paper

Simple computer code for estimating cosmic-ray shielding by oddly shaped objects

Greg Balco*

Berkeley Geochronology Center, 2455 Ridge Road, Berkeley, CA 94709, USA

ARTICLE INFO

Article history:
Received 5 October 2013
Received in revised form
18 December 2013
Accepted 20 December 2013
Available online 1 January 2014

Keywords:
Cosmogenic nuclide geochemistry
Exposure-age dating
Monte Carlo integration
Precariously balanced rocks

ABSTRACT

This paper describes computer code for estimating the effect on cosmogenic-nuclide production rates of arbitrarily shaped obstructions that partially or completely attenuate the cosmic ray flux incident on a sample site. This is potentially useful for cosmogenic-nuclide exposure dating of geometrically complex landforms. The code has been validated against analytical formulae applicable to objects with regular geometries. It has not yet been validated against empirical measurements of cosmogenic-nuclide concentrations in samples with the same exposure history but different shielding geometries.

1. Importance of geometric shielding of the cosmic-ray flux to exposure dating

Cosmogenic-nuclide exposure dating is a geochemical method used to determine the age of geological events that modify the Earth's surface, such as glacier advances and retreats, landslides, earthquake surface ruptures, or instances of erosion or sediment deposition. To determine the exposure age of a rock surface, one must i) measure the concentration of a trace cosmic-ray-produced nuclide (e.g., ^{10}Be, ^{26}Al, ^{3}He, etc.); and ii) use an independently calibrated nuclide production rate to interpret the concentration as an exposure age (see review in Dunai, 2010).

Typically (Dunai, 2010), estimating the production rate at a sample site employs simplifying assumptions that i) the sample is located on an infinite flat surface; ii) all cosmic rays responsible for nuclide production originate from the upper hemisphere; and iii) any topographic obstructions to the cosmic-ray flux can be represented as an apparent horizon below which cosmic rays are fully obstructed, and above which they are fully admitted (the 'opaque-horizon' assumption). These assumptions are adequate for a wide range of useful exposure-dating applications, but they fail for sample sites located on irregular surfaces with a roughness scale similar to the characteristic cosmic ray attenuation length in rock (order 1 m), or likewise for sample sites located on or near meter-scale boulders or other objects.

The opaque-horizon assumption fails in these situations for two reasons. First, rock is denser than air. Attenuation of cosmic rays is proportional to the amount of mass they travel through. Thus, if cosmic rays must penetrate both the overlying atmosphere and also some additional thickness of rock (or any massive material, e.g., soil, sediment, water, etc.) to reach a sample site, then the production rate at that site will be less than it would be in the reference case of an infinite flat surface (where cosmic rays only travel through air to reach the sample site). If the thickness of rock traversed is much longer than the cosmic-ray attenuation length (e.g., tens of meters or more), then the cosmic-ray flux from that direction is completely attenuated and the opaque-horizon assumption is adequate. However, if it is relatively short (order 1 m) then the cosmic-ray flux is only partially attenuated and this assumption fails. This effect is referred to in this paper as 'geometric shielding.' The term 'self-shielding' is sometimes used to describe this effect, although that term is somewhat misleading because both the rock that is being sampled ('self') and other nearby objects could shield the sample site.

Second, a fraction of cosmogenic-nuclide production at a sample site near the Earth's surface is due to secondary particles that originate in nuclear reactions relatively close to the sample site. Because the mean atomic weight of rock is greater than that of air, and also because air is less dense than rock so it is more likely that some particles will decay before interacting, the yield of these secondary particles is greater from rock that from air. Thus, when a

* Tel.: +1 510 644 9200; fax: +1 510 644 9201.
E-mail address: balcs@bgc.org.

1871-1014/$ – see front matter © 2014 Elsevier B.V. All rights reserved.
http://dx.doi.org/10.1016/j.quageo.2013.12.002

sample is surrounded by more air, and less rock, than it would be if it was embedded in the reference infinite flat surface – for example if it lies on a steeply dipping surface, or within a relatively small boulder – then the flux of these secondary particles, and therefore the production rate, is correspondingly less. This effect is referred to here as the 'missing mass effect;' Masarik and Wieler (2003) also called it the 'shape effect.'

The magnitude of the geometric shielding effect can vary from negligible to complete attenuation depending on the arrangement and size of obstructions. The magnitude of the missing mass effect is expected to be at most ~10% of the production rate (i.e., for the extreme case in which a sample lies at the top of a tall, thin pillar; Masarik and Wieler, 2003). Thus, in many common geomorphic situations, geometric shielding is expected to be significantly more important (a tens-of-percent-level effect on the production rate) than the missing mass effect (a percent-level effect). Geometric shielding is also easier to calculate. The remainder of this paper describes computer code that computes geometric shielding for arbitrary geometry of samples and obstructions; this calculation only requires determining the lengths of ray paths that pass through objects and applying an exponential attenuation factor to each ray path. Computer code to implement this is simple and fast enough to permit, for example, dynamic calculation of shielding factors in a model where the shielding geometry evolves during the exposure history of a sample. Previous attempts to quantify the missing mass effect, on the other hand, have employed a complete simulation of the cascade of nuclear reactions in the atmosphere and rock that give rise to the particle flux at the sample site, using first-principles particle interaction codes such as MCNP or GEANT (Masarik and Beer, 1999, and references therein). These codes are slow, complex, and require extensive computational resources. To summarize, because of the difference in the potential magnitude of these two effects, there are likely to be many geomorphically relevant situations involving samples with complicated shielding geometry in which one can estimate production rates at useful (i.e., percent-level) accuracy using only the relatively simple geometric shielding calculation. The calculations in this paper consider only the geometric shielding effect and do not consider the missing mass effect. A valuable future contribution would be to develop a simplified method of approximating the missing mass effect using only geometric considerations that would not require complex particle physics simulation code.

Although both the geometric shielding effect and the missing mass effect follow from well-established physical principles, there has been very little attempt to verify calculations of these effects by measuring cosmogenic-nuclide concentrations in natural situations where they are expected to be important. For example, simulations of the missing mass effect predict a relationship between boulder size, sample location on a boulder, and cosmogenic-nuclide concentration. Although some researchers have argued that this relationship is or is not present in certain exposure-age data sets (Masarik and Wieler, 2003; Balco and Schaefer, 2006), the scatter in the data sets is similar in magnitude to expected effects, so these results were ambiguous. Kubik and Reuther (2007) attempted to conduct a better constrained experiment by matching cosmogenic ^{10}Be concentrations measured on and beneath a cliff surface, where both geometric shielding and missing mass effects would be expected to be important, with model estimates of these effects. However, they were not able to reconcile observations with predictions at high confidence. One purpose of this paper is to facilitate future attempts to validate geometric shielding factor estimates by simplifying the calculation of shielding factor estimates for irregular shapes characteristic of natural outcrops or boulders.

The computer code described in this paper was originally developed for exposure-dating of precariously balanced rocks used in seismic hazard estimation. These rocks are 1–2 m in size and irregular in shape (e.g., Fig. 1), so most sample locations are partially shielded by the rocks themselves. To quantify these effects, in Balco et al. (2011) we developed computer code to calculate geometric shielding factors for arbitrarily shaped objects. However, that paper did not include the code or describe it in detail. The present paper provides a complete description and includes the code as supplementary information. In addition, the code and accompanying documentation are available online at http://hess.ess.washington.edu/shielding.

2. Definition of geometric shielding; previous work

The treatment of geometric shielding in this paper follows that of Lal (1991), which was also adopted by Dunne et al. (1999), Lal and Chen (2005), and Mackey and Lamb (2013). Dunne et al. (1999) provide a complete and clear derivation of the following equations. Cosmic ray intensity as a function of direction $I(\theta,\phi)$, where θ is the zenith angle measured down from the vertical and ϕ is the azimuthal angle, is assumed to be constant in azimuth but vary with zenith angle, such that:

$$I(\theta,\phi) = I_0 \cos^m(\theta) \quad (1)$$

I_0 is the maximum intensity (in the vertical direction) and the value of m has been estimated from cosmic-ray observations and is generally taken to be 2.3 (see Gosse and Phillips, 2001, for additional discussion). The total flux F_{ref} that an object receives in the reference case of full exposure to the entire upper hemisphere, that is, when a sample site is located on an infinite, unshielded, flat surface, is:

$$F_{\mathrm{ref}} = I_0 \int_{\phi=0}^{2\pi} \int_{\theta=0}^{\pi/2} \cos^m(\theta)\sin(\theta)\,\mathrm{d}\theta\,\mathrm{d}\phi \quad (2)$$

This can be evaluated analytically with the result that:

$$F_{\mathrm{ref}} = I_0 \frac{2\pi}{m+1} \quad (3)$$

Intensity I would typically have units of particles cm^{-2} sr^{-1} s^{-1}. However, the purpose of this work is to calculate a dimensionless shielding factor that is the ratio of the production rate at a shielded site to that at an identically located unshielded site, so neither the units nor the absolute value of I or F_{ref} are relevant.

Geometric shielding is here defined to be the integrated shielding effect of any objects more dense than air that cosmic rays must traverse to reach a sample site. This depends on the size and location of nearby objects relative to the sample. Geometric shielding of the cosmic-ray flux from a particular direction, incident on a particular sample location, can be represented as the mass thickness traversed by cosmic rays from that direction before they reach the sample. This mass thickness is $\rho r(x,y,z,\theta,\phi)$ and has units of g cm^{-2}. ρ is the mean density of the material traversed by the cosmic rays (g cm^{-3}). $r(x,y,z,\theta,\phi)$ is the linear thickness (cm) of this material that a cosmic ray arriving from zenith angle θ and azimuth ϕ must traverse to reach a sample site whose location is defined by Cartesian coordinates x, y, and z. Attenuation of cosmic rays traveling in a particular direction is then defined to be exponential in mass thickness with a constant attenuation length Λ_p, such that if the intensity of the incoming cosmic-ray flux in that direction is I and the intensity of the cosmic ray flux in that direction at the sample site is I_s, then $I_s/I = \exp(-\rho r/\Lambda_p)$. Note that Λ_p, which represents an attenuation length along a single incidence direction for

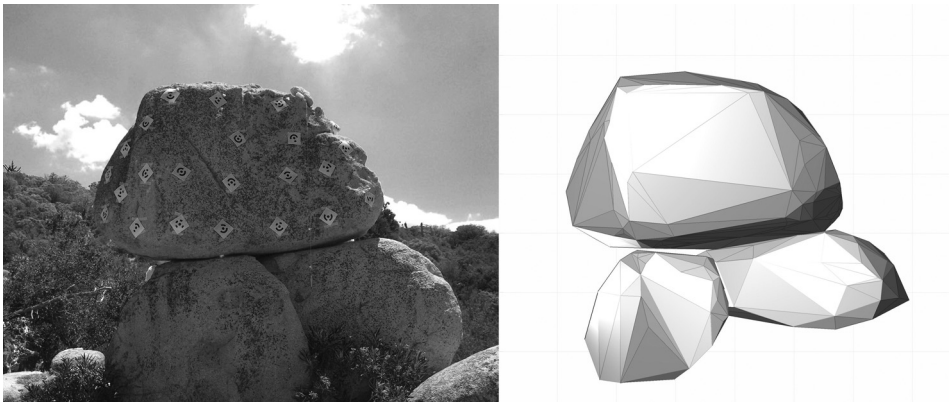

Fig. 1. Photograph and shape model of a precariously balanced rock in southern California, USA (Balco et al., 2011). The shape model was photogrammetrically generated: tape markers (visible in photo) were attached to the rock, the rock was photographed from multiple directions, and the software package Photomodeler was used to generate a representation of the rock as a set of triangular facets.

cosmic rays with energies appropriate for inducing spallation reactions in rock, differs from the apparent attenuation length for total spallogenic cosmic-ray production with depth below an infinite flat surface, which is commonly used in exposure-dating calculations and is usually denoted as Λ. Dunne et al. (1999) showed that for constant Λ_p and $m = 2.3$, $\Lambda_p \simeq 1.3\,\Lambda$.

Thus, the cosmic-ray flux at a sample location (x,y,z) subject to geometric shielding is:

$$F = I_0 \int_{\phi=0}^{2\pi} \int_{\theta=0}^{\pi/2} \cos^m(\theta)\sin(\theta) e^{-\frac{\rho r(x,y,z,\theta,\phi)}{\Lambda_p}} \mathrm{d}\theta\,\mathrm{d}\phi \quad (4)$$

The dimensionless shielding factor for that sample location relative to an unshielded sample is then F/F_{ref}. Computing this requires evaluating the integral in Equation (4), which in turn requires computing the attenuation pathlength $r(x,y,z,\theta,\phi)$ for arbitrary sample location and cosmic ray incidence direction.

This approach to computing geometric shielding is routinely used in nuclear physics to compute fluxes of particles that are simply absorbed in exponential proportion to mass traversed, for example in calculating x- or gamma-ray penetration in objects. As discussed above, however, when applied to calculate shielding factors for high-energy cosmic-ray spallation, it disregards the fact that cosmic ray interactions within rock may yield secondary particles that themselves could contribute to nuclide production. In addition, the assumption of constant Λ_p is an important simplification. In reality, the attenuation length for cosmic rays depends on their energy. The energy spectrum of cosmic rays varies with location in the Earth's atmosphere and magnetic field as well as with zenith angle, so Λ_p is also expected to be a function of these parameters. In addition, different nuclides of interest are produced by reactions with different threshold energies, so a single value of Λ_p is not expected to be appropriate for all nuclides. Although in this code we have disregarded these effects by assuming constant Λ_p, if theoretical predictions of neutron energy spectra, their variation with zenith angle, and the corresponding variations in effective attenuation length were available for a given sample location (presumably from a first-principles particle physics simulation), the code could easily be modified to include variable Λ_p, or to integrate over an energy spectrum in addition to solid angle (the MATLAB code is commented to this effect in the appropriate locations).

This code is not appropriate for describing attenuation of the cosmic-ray muon flux. However, the effective attenuation length for muons in rock is an order of magnitude or more longer than that for high-energy neutrons, so the effect of meter-scale surface obstructions on production rates due to muons is expected to be negligible.

Several previous authors have computed shielding factors using the assumptions and formulae described above for regular geometries where attenuation path lengths r can be represented by analytical functions of x, y, z, ϕ, and θ. Dunne et al. (1999) computed shielding factors at and below flat and dipping surfaces subject to complete obstruction of the cosmic-ray flux from some fraction of the upper hemisphere. Lal and Chen (2005) also computed shielding factors below dipping surfaces, and in addition for the interior of spherical and cubic boulders. Mackey and Lamb (2013) considered spheres. However, natural rock landforms that one might wish to exposure date are commonly irregularly shaped, which requires a numerical integration method. The method described here uses Monte Carlo integration to evaluate the integral and a ray-tracing method, applied to a representation of the shielding objects as a set of triangular facets, to compute the path lengths. This approach is similar to that used by Plug et al. (2007) to compute the cosmic-ray shielding effect of a forest.

3. Description of computer code

The computer code described in this paper is written in MATLAB, a high-level programming language designed for mathematical computation and commonly used by Earth scientists. Several other computational tools for cosmogenic-nuclide production rate calculations are also written in MATLAB (Balco et al., 2008; Goehring et al., 2010). The typical workflow for using this code would be as follows: First, generate a shape model for the objects of interest. Typically one would use a photogrammetric method or a laser scanning system to do this. Second, locate sample locations in the same coordinate system as the shape model. Finally, use the code supplied here to estimate geometric shielding at the sample site by Monte Carlo integration.

3.1. Shape models

A "shape model" as used here is a set of triangular facets that enclose one or more volumes (Fig. 1). Typically, one would define a shape model so that the facets form a closed irregular polyhedron for each obstruction. However, one could also define a set of facets that did not form a closed volume, for example to represent a cliff face or hillside.

This code reads in shape files defined in the ASCII .stl file format.[1] "STL" stands for "standard tesselation language." This file format is commonly used in 3-D modeling software, 3-D printing, and computer-aided design and manufacturing. The file begins with a line defining the name of the solid, and is followed by a series of line groups, each of which defines the vertices of a triangular facet. An example of a .stl file defining two facets is as follows:

```
solid [/Users/balcs/shielding_calcs/temp.stl]
facet normal 0.00 0.00 0.00
  outer loop
    vertex      -4.957786      -2.770371       0.602929
    vertex      -4.896107      -2.830239       0.808729
    vertex      -4.975159      -2.737364       0.196783
  endloop
endfacet
facet normal 0.00 0.00 0.00
  outer loop
    vertex      -5.194063      -3.575649      -0.017283
    vertex      -5.434190      -3.412690      -0.130366
    vertex      -5.042836      -3.470916      -0.059296
  endloop
endfacet
endsolid
```

Each line beginning with 'vertex' contains the x, y, and z coordinates of one of the vertices of the facet. In general, a .stl file contains no scale information and the units are arbitrary. This code assumes that the coordinates of the vertices have units of meters. The three values in each line beginning with 'facet normal' are intended to define the unit normal vector of each facet. However, as this information is redundant with the coordinates of the vertices, many software packages dealing with .stl files (including this one) ignore values in these positions or insert zeros. In some implementations of .stl files, the order of the vertices indicates 'inside' and 'outside' sides of each facet, i.e., the vertices are defined in clockwise order when viewed from the outside of the object. The order of the vertices is ignored here. A binary version of the .stl file format exists, but is not supported here.

In previous work (Balco et al., 2011) we used the photogrammetric software Photomodeler (www.photomodeler.com) to generate .stl files describing precariously balanced boulders that were the subject of an exposure-dating study. Fig. 1 shows an example. Many commercial and open-source software packages with similar capabilities exist.

3.2. Path length calculation

A shape model is a collection of sets of three [x,y,z] triples, each set defining a facet. Given this information and the coordinates of a sample location in the same coordinate system, the thickness of rock traversed by a cosmic ray with arbitrary direction is calculated using the following algorithm.

1. *Change coordinates*. Shift the coordinates of the shape model and sample location so that the sample location is at coordinates [0,0,0]. That is, if a vertex as originally defined in the shape model has coordinates [a,b,c] and the sample location as originally defined has coordinates [a_s,b_s,c_s], transform them to new coordinates [x,y,z] where $x = a - a_s$, $y = b - b_s$, and $z = c - c_s$. Basically, the effect of this transformation is to represent each vertex in the shape model as a vector originating at the sample site.
2. *Find intersections between a cosmic ray and each facet in the shape model*. In the sample-centered coordinate system, the vector representing a cosmic ray incident on the sample location is a linear combination of the vectors representing the corners of any facet. If the vector representing a cosmic ray incidence direction has coordinates x_r, y_r, and z_r, and the three vertices of the facet have coordinates x_i, y_i, and z_i where $i = 1...3$, then:

$$\begin{bmatrix} x_1 & x_2 & x_3 \\ y_1 & y_2 & y_3 \\ z_1 & z_2 & z_3 \end{bmatrix} \begin{bmatrix} p \\ q \\ r \end{bmatrix} = \begin{bmatrix} x_r \\ y_r \\ z_r \end{bmatrix} \quad (5)$$

This is useful because if p, q, and r are all greater than zero, then the cosmic ray passes through the facet. Thus, solving Equation (5) for each facet enables one to identify those facets that the ray passes through. Fig. 2 shows an example. In principle this is computationally inefficient because one must consider all facets for each cosmic ray, so computation time scales linearly with the number of facets in the shape model. However, for typical shape models with hundreds of facets, it is fast enough for this purpose.
3. *Calculate the path distances in rock*. Having identified the facets in the shape model that the ray passes through, one can compute i) the points of intersection between the ray and each facet, and ii) the distance between each intersection point and the sample location. If there are a large number of objects in the shape model, then there could be many such intersection points. This requires some way of determining which sections of the ray path are inside objects and which are outside. The algorithm to accomplish this involves assuming that the sample location is

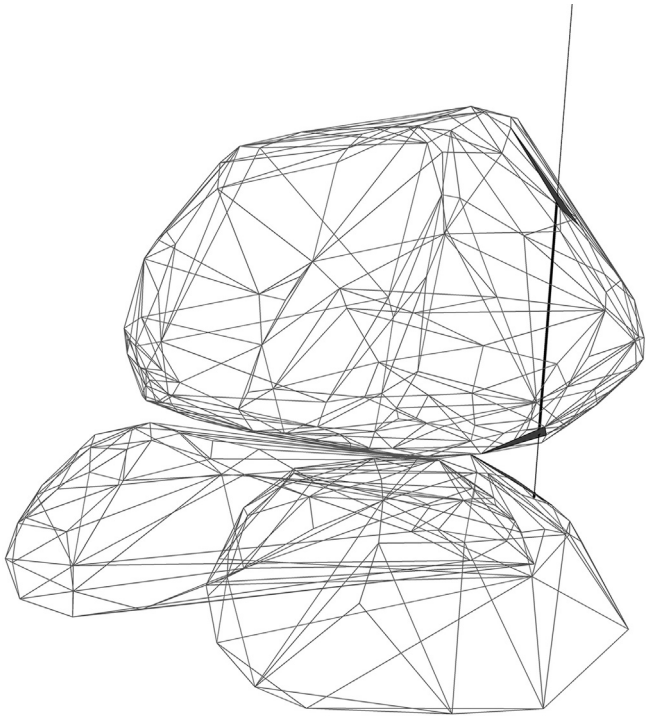

Fig. 2. Intersection of a representative cosmic ray path with the shape model shown in Fig. 1. The shape model is shown as a wireframe mesh. A near-vertical cosmic ray path to a sample location on the pedestal below the precariously balanced rock enters the top of the rock, exits the bottom of the rock, and enters the pedestal to reach the sample location. Facets that intersect the ray path are highlighted by gray fill. The portion of the cosmic ray path that traverses rock is highlighted by a thickened line.

[1] e.g., http://en.wikipedia.org/wiki/STL_(file_format).

within an object. In reality, this should always the case for an exposure-dating application because the sample collected for analysis has some thickness greater than zero, and the production rate calculation applies to the shape of the object before the sample was removed. Thus, the center of the sample where one wishes to compute the production rate is, by definition, inside an object. In the simplest case where the shape model contains a single convex object, then any cosmic ray can only intersect one facet, where it enters the object on its way to the sample location. In a more complicated case including a single non-convex object or many objects, then the ray can enter or exit many different objects, or the same object multiple times, intersecting $2n + 1$ facets where n is the number of additional objects intersected (or the number of crossings of one complex object). Thus, one can determine which sections of the ray path lie within rock by sorting the intersection points according to distance from the sample location and assuming that the pathlength between the sample and the closest intersection is rock, the pathlength between the closest and second-closest intersections is air, the pathlength between the second-closest and third-closest intersections is rock, and so on. See Fig. 2. Note that this algorithm assumes that all objects are closed shapes, which implies that there will always be an odd number of intersections. An even number of intersections could only arise from a topological error in defining the objects in the shape model. However, in practice it might be potentially useful to define some non-closed shapes in a shape model to represent objects that are large enough to fully stop the cosmic-ray flux, e.g., cliff faces or hillsides. To accommodate this, the code provides an option to assume that an even number of intersections signals total attenuation of a particular cosmic ray.

In applying this method to exposure dating of precariously balanced rocks in Balco et al. (2011), we also allowed for the possibility that objects were embedded in soil whose surface lay above the sample site. This can be accounted for by computing the intersection between the cosmic ray and a horizontal soil surface, disregarding all cosmic ray-facet intersections that lie below the soil surface, and applying the algorithm in (3) above to the intersection with the soil surface and any remaining ray-facet intersections.

3.3. Monte Carlo integration

The algorithm described above applied to a shape model enables one to compute $r(x,y,z,\theta,\phi)$. This permits numerical integration of Equation (4) by Monte Carlo integration. Monte Carlo integration is a method of estimating the integral of a function over some region by generating a uniformly distributed random sample of points within the region and computing the value of the function at those points. In general, given a function of two variables x and y to be integrated over a region $0 \le x \le a$ and $0 \le y \le b$,

$$I_{MC} = \frac{ab}{N}\sum_{i=1}^{N} f(x_i, y_i) \simeq \int_0^b \int_0^a f(x,y)\,dx\,dy \quad (6)$$

where I_{MC} is the Monte Carlo estimate of the integral, N is the number of points in the sample, and the sample points are uniformly distributed in x and y and have coordinates (x_i,y_i). Thus, the Monte Carlo estimate for the geometric shielding factor F/F_{ref} for a sample with coordinates (x,y,z) is:

$$\left(\frac{2\pi}{m+1}\right)^{-1}\frac{\pi^2}{N}\sum_{i=1}^{N}\cos^m(\theta_i)\sin(\theta_i)e^{-\frac{\rho r(x,y,z,\theta_i,\phi_i)}{\Lambda_\rho}} \quad (7)$$

for N sample points (θ_i,ϕ_i) that are uniformly distributed in ϕ and θ.

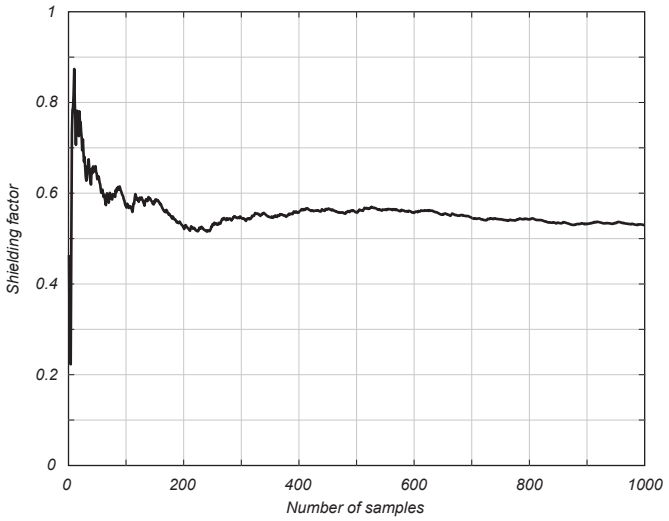

Fig. 3. Example of convergence of the Monte Carlo integration estimate of the shielding factor (for the sample location shown in Fig. 2) as the sample size increases. Typically the shielding factor converges on a stable value after ~500 iterations.

The number of sample points needed for an accurate Monte Carlo estimate of the geometric shielding factor depends on the geometry. There exist formal methods of estimating the uncertainty in a Monte Carlo integral based on the convergence of the results, but they are not included in the present code. Note that because this calculation includes systematic uncertainties that stem from the simplifying assumptions discussed above, the formal uncertainty of the Monte Carlo estimate is not expected to accurately represent the true uncertainty in the shielding factor. One can informally estimate the required sample size by successively increasing the number of sample points and determining when the resulting shielding factor converges on a stable and reproducible value. Fig. 3 shows an example. In the application to precariously

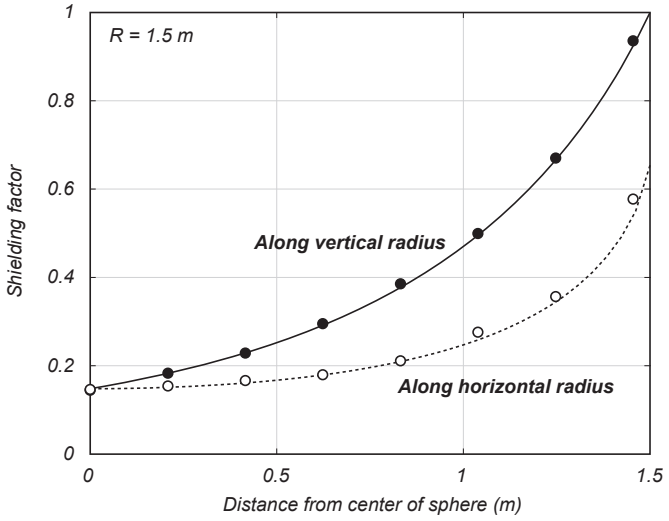

Fig. 4. Validation of Monte Carlo integration code against analytical formulae of Lal and Chen (2005) for geometric shielding factors inside a hemispherical boulder with radius 1.5 m. The solid and dashed lines are analytical results for samples along vertically-oriented and horizontally-oriented, respectively, radii, and in part reproduce Figure 4 of Lal and Chen (2005). The circles show shielding factors at the same locations calculated by the Monte Carlo integration with $N = 1000$. MATLAB code to generate this figure is included in the supplemental information.

balanced rocks, we found that $N \simeq 500$ was nearly always sufficient.

3.4. Validation against analytical results

I attempted to validate this code by comparing it to analytical formulae, computed by other authors, for the integral in Equation (4) applied to simple geometries. First, Lal and Chen (2005) derived formulae for computing the geometric shielding factor at points within spherical boulders. In this situation, the cosmic-ray flux is partially attenuated by passing through the boulder itself. Fig. 4 shows that the Monte Carlo integration yields the same results as their formulae. Second, Dunne et al. (1999) derived formulae for computing shielding due to complete obstruction of portions of the upper hemisphere. This case differs from the ones considered by Lal and Chen (2005) and Balco et al. (2011) because it does not involve partial attenuation of the cosmic-ray flux from certain directions, only total obstruction. However, the results of Dunne and others are a useful test of this code because they describe not only a shielding factor at the surface due to an obstructed horizon, but also the effect that the cosmic-ray flux is more vertically collimated when the horizon is obstructed than when it is not, so the depth-dependence of the production rate varies between these cases. The Monte Carlo integration can be used to simulate this effect, and Fig. 5 shows that it correctly reproduces the Dunne et al. results.

3.5. Validation against measurements

In principle, one could validate shielding factors estimated with this code by comparing them to measured cosmogenic-nuclide concentrations in natural samples. This would require i) an irregularly shaped object with meter-scale dimensions that was emplaced with zero concentration of cosmic-ray-produced nuclides and subsequently exposed to the cosmic-ray flux without any change in its geometry, ii) a shape model of the object, and iii) measurements of nuclide concentrations from multiple locations on that object that have different degrees of geometric shielding. In this case the cosmogenic-nuclide concentrations will be directly proportional to the true shielding factors, allowing straightforward validation of shielding factor estimates. These conditions could be satisfied, for example, by sampling several locations on and/or within a glacially transported moraine boulder. However, because nearly all exposure-dating studies seek to avoid complicated geometric shielding calculations by sampling only from the top of boulders or outcrops, I am not aware of any such data set.

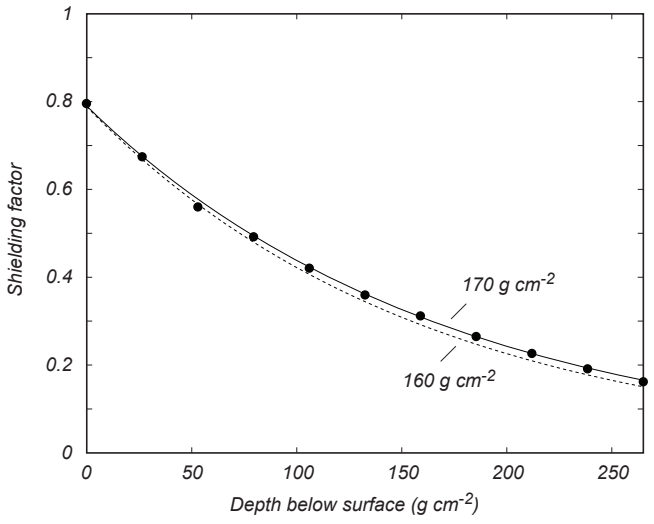

Fig. 5. Validation of Monte Carlo integration against calculations by Dunne et al. (1999) of production rates on and beneath a flat surface obstructed by a thick obstacle spanning an azimuth of 180° and horizon angle of 50°. The obstructed horizon both reduces the production rate at the surface relative to that for an unshielded surface (by a factor of 0.79 in this example) and also causes the cosmic-ray flux at the site to be more vertically collimated, which increases the apparent attenuation length for subsurface production. The dark line shows shielding factors (the production rate relative to the production rate on an unshielded flat surface at the same location) predicted by Dunne et al. (1999) for this horizon geometry, and the circles show equivalent shielding factors predicted by the Monte Carlo integration with $N = 2000$. The dashed line shows an exponential depth dependence with the shorter attenuation length expected for an unshielded surface (here 160 g cm^{-2}) to highlight the fact that the Monte Carlo results correctly reproduce the attenuation length prediction of Dunne et al. MATLAB code to generate this figure is included in the supplemental information.

Studies of precariously balanced rocks in Balco et al. (2011) and other more recent research (e.g., Rood et al., 2012) collected data that meets some, but not all, of these requirements. These data include photogrammetric shape models of irregularly shaped rocks with meter-scale dimensions, and multiple ^{10}Be measurements at different locations on these rocks. However, it is not straightforward to use these data to evaluate the accuracy of shielding factor calculations because the rocks were exhumed by downwasting of regolith (and the exhumation history is not known independently of the ^{10}Be measurements), so all the samples did not have the same exposure history, and the shielding geometry changed through time. However, these studies were able to closely match measured ^{10}Be concentrations with a model for ^{10}Be production during rock exhumation that was based on shielding factors computed using the Monte Carlo integration code described here. Fig. 6 shows an example from Rood et al. (2012). Calculated shielding factors for samples from this rock vary by a factor of four (from 0.2 to 0.8), and, as shown in Fig. 6, variations in measured ^{10}Be concentrations have similar pattern and magnitude. Thus, an exhumation history could be found (using the method of Balco et al., 2011) that was consistent with geomorphic constraints, ^{10}Be concentrations, and shielding factor estimates. Because the forward model includes additional assumptions besides the shielding factor estimates, this comparison does not directly validate the shielding factor estimates. However, given the large variation in shielding factor among these samples, it would be difficult to match measured nuclide concentrations if the shielding factor estimates were highly inaccurate. Again, a better approach to this would be to make similar measurements on a boulder with a simple exposure history. This would be a valuable future contribution.

4. Example uses

The general purpose of the Monte Carlo integration code is to permit exposure-dating of samples that are surrounded by meter-scale surface obstructions. In many common exposure-dating situations, for example exposure-dating of glacially transported boulders, complex shielding calculations of this sort are, of course, mostly not necessary because it is easier to select unshielded sample sites. The reason this code was developed for reconstructing exhumation histories of precariously balanced rocks useful in seismic hazard analysis is because sampling only unshielded parts of these features did not provide enough information to determine when they were formed. The fact that the shielding geometry changes as the rocks are exhumed required a relatively simple and quick method of estimating not only present geometric shielding factors but also changes in the shielding factor over time. Fig. 7 shows an example calculation for this application, and MATLAB code to generate these results is included in the supplemental material.

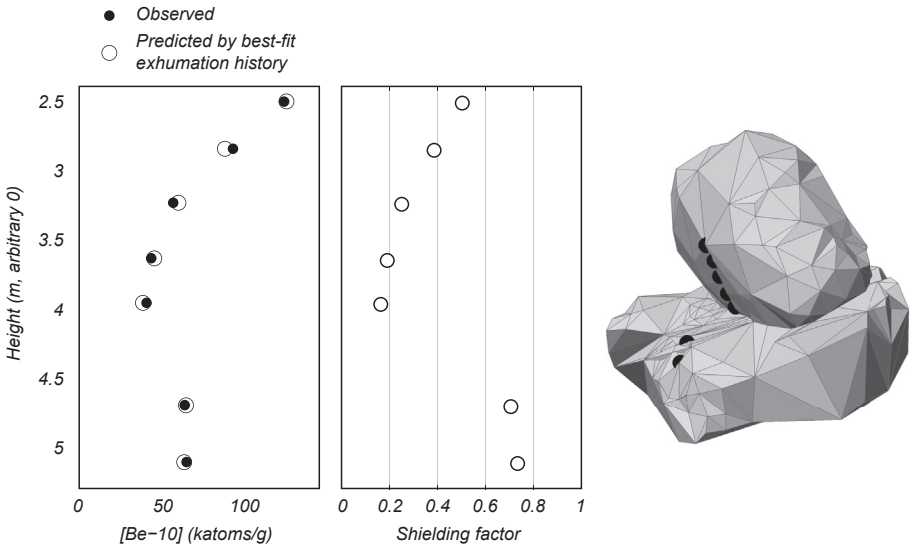

Fig. 6. The right-hand panel shows a shape model for a precariously balanced rock near Lake Los Angeles, CA, described by Rood et al. (2012). Black circles show sample locations. The center panel shows geometric shielding factors calculated by Monte Carlo integration for these samples. The left panel shows cosmogenic ^{10}Be concentrations measured by Rood et al. (2012) in these samples (black circles) as well as ^{10}Be concentrations predicted by a forward model based on these shielding factors and a best-fitting exhumation history (using the method of Balco et al., 2011) (open circles).

Other obvious applications include estimating erosion rates where soil erosion leads to progressive exposure of rock features such as tors (e.g., Heimsath et al., 2000), or to estimate when features like arches or sea stacks were formed by cliff retreat. More complex applications would include attempting to determine the frequency of boulder transport by comparing measured cosmogenic-nuclide concentrations to present shielding geometries (Mackey and Lamb, 2013); or, potentially, archeological applications aimed at verifying that sculpture or stonework has resided in its present geometric configuration since constructed.

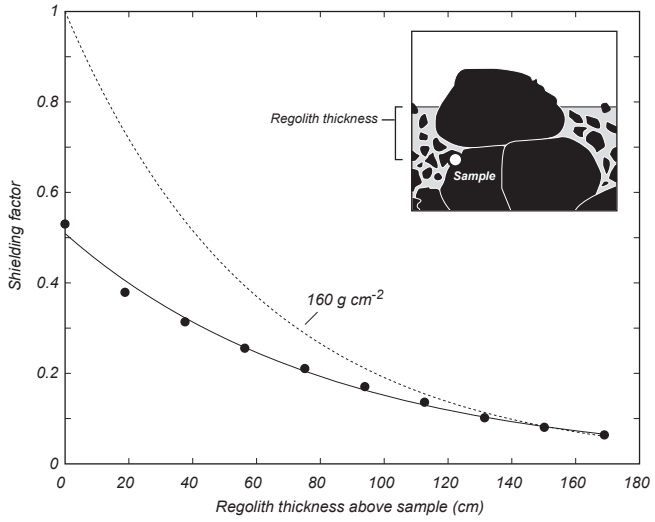

Fig. 7. Example calculation showing the variation in shielding factor for the sample shown in Fig. 2 with increasing thickness of regolith above the sample location. This reproduces the calculation of Balco et al. (2011) (also note correction in Balco et al., 2012). The black circles are the results of the Monte Carlo integration with $N = 1000$. The solid line shows an exponential function fit to the Monte Carlo results; this fitting procedure is used to derive the sample-specific constants $S_{0,i}$ and L_i in Table 1 of Balco et al. (2011). The dashed line shows the variation in spallogenic production rate with depth below the surface expected for an infinite flat surface (exponentially decreasing with an attenuation length of 160 g cm^{-2}). The top of the precariously balanced rock is 169 cm above the sample, so when the sample is covered by 169 cm of regolith, the PBR no longer protrudes above the surface and the sample experiences the same shielding that it would ordinarily experience below a flat surface. MATLAB code to generate this figure is included in the supplemental information.

Acknowledgments

Dylan Rood provided the impetus for this work by telling me about precariously balanced rocks in the first place. This work was supported in part by the Ann and Gordon Getty Foundation.

Editorial handling by: D. Bourles

Appendix A. Supplementary material

Supplementary data related to this article can be found at http://dx.doi.org/10.1016/j.quageo.2013.12.002.

References

Balco, G., Purvance, M., Rood, D., 2011. Exposure dating of precariously balanced rocks. Quat. Geochronol. 6, 295–303.
Balco, G., Purvance, M., Rood, D., 2012. Corrigendum to "Exposure dating of precariously balanced rocks" [Quaternary Geochronology 6 (2011) 295–303]. Quat. Geochronol. 9, 86.
Balco, G., Schaefer, J., 2006. Cosmogenic-nuclide and varve chronologies for the deglaciation of southern New England. Quat. Geochronol. 1, 15–28.
Balco, G., Stone, J., Lifton, N., Dunai, T., 2008. A complete and easily accessible means of calculating surface exposure ages or erosion rates from ^{10}Be and ^{26}Al measurements. Quat. Geochronol. 3, 174–195.
Dunai, T., 2010. Cosmogenic Nuclides: Principles, Concepts, and Applications in the Earth Surface Sciences. Cambridge University Press, Cambridge, UK.
Dunne, J., Elmore, D., Muzikar, P., 1999. Scaling factors for the rates of production of cosmogenic nuclides for geometric shielding and attenuation at depth on sloped surfaces. Geomorphology 27, 3–12.
Goehring, B., Kurz, M., Balco, G., Schaefer, J., Licciardi, J., Lifton, N., 2010. A reevaluation of in-situ cosmogenic He-3 production rates. Quat. Geochronol. 5, 410–418.
Gosse, J.C., Phillips, F.M., 2001. Terrestrial in situ cosmogenic nuclides: theory and application. Quat. Sci. Rev. 20, 1475–1560.
Heimsath, A., Chappell, J., Dietrich, W., Nishiizumi, K., Finkel, R., 2000. Soil production on a retreating escarpment in southeastern Australia. Geology 28 (9), 787–790.
Kubik, P., Reuther, A., 2007. Attenuation of cosmogenic ^{10}Be production in the first 20 cm below a rock surface. Nucl. Instrum. Methods Phys. Res. B 259, 616–624.
Lal, D., 1991. Cosmic ray labeling of erosion surfaces: in situ nuclide production rates and erosion models. Earth Planet. Sci. Lett. 104, 424–439.
Lal, D., Chen, J., 2005. Cosmic ray labeling of erosion surfaces II: special cases of exposure histories of boulders, soil, and beach terraces. Earth Planet. Sci. Lett. 236, 797–813.

Mackey, B., Lamb, M., 2013. Deciphering boulder mobility and erosion from cosmogenic nuclide exposure dating. J. Geophys. Res. Earth Surf. 118, 184–197.
Masarik, J., Beer, J., 1999. Simulation of particle fluxes and cosmogenic nuclide production in Earth's atmosphere. J. Geophys. Res. 104, 12099–12111.
Masarik, J., Wieler, R., 2003. Production rates of cosmogenic nuclides in boulders. Earth Planet. Sci. Lett. 216, 201–208.
Plug, L., Gosse, J., McIntosh, J., Bigley, R., 2007. Attenuation of cosmic ray flux in temperate forest. J. Geophys. Res. 112, F02022.
Rood, D., Anooshehpoor, R., Balco, G., Biasi, G., Brune, J., Brune, R., Grant Ludwig, L., Kendrick, K., Purvance, M., Saleeby, I., 2012. Testing seismic hazard models with Be-10 exposure ages for precariously balanced rocks. In: American Geophysical Union 2012 Fall Meeting, San Francisco, CA. Abstract 1493571.